Enhanced electric field sensitivity of rf-dressed Rydberg dark states

2010 New J. Phys. 12 065015

(http://iopscience.iop.org/1367-2630/12/6/065015)

New Journal of Physics
The open-access journal for physics

Enhanced electric field sensitivity of rf-dressed Rydberg dark states

M G Bason[1], M Tanasittikosol[1,4], A Sargsyan[2], A K Mohapatra[3], D Sarkisyan[2], R M Potvliege[1] and C S Adams[1]

[1] Department of Physics, Durham University, Rochester Building, South Road, Durham DH1 3LE, UK
[2] Institute for Physical Research, Armenia National Academy of Science, 0203 Ashtarak-2, Armenia
[3] 5. Physikalisches Institut, Universität Stuttgart, Pfaffenwaldring 57, 70569 Stuttgart, Germany
E-mail: monsit.tanasittikosol@durham.ac.uk

New Journal of Physics **12** (2010) 065015 (11pp)
Received 2 November 2009
Published 28 June 2010
Online at http://www.njp.org/
doi:10.1088/1367-2630/12/6/065015

Abstract. Optical detection of Rydberg states using electromagnetically induced transparency (EIT) enables continuous measurement of electric fields in a confined geometry. In this paper, we demonstrate the formation of radio frequency (rf)-dressed EIT resonances in a thermal Rb vapour and show that such states exhibit enhanced sensitivity to dc electric fields compared to their bare counterparts. Fitting the corresponding EIT profile enables precise measurements of the dc field independent of laser frequency fluctuations. Our results suggest that space charges within the enclosed cell reduce electric field inhomogeneities within the interaction region.

[4] Author to whom any correspondence should be addressed.

Contents

1. Introduction

Rydberg atoms are interesting in the context of precision measurement and sensing because of their strong interatomic interactions and extreme sensitivity to electric fields [1]. The application of Rydberg states as electric field sensors has been explored using a supersonic beam of krypton atoms with principal quantum number $n = 91$ [2]. This experiment demonstrates the potential for electrometry using highly excited Rydberg states with a measured sensitivity of 20 μV cm^{-1}. However, a disadvantage of using Rydberg atoms is that the standard detection technique of pulsed field ionization means that the measurement cannot be performed continuously, and typically the detection system is relatively large. Recently, the coherent optical detection of Rydberg states using electromagnetically induced transparency (EIT) was demonstrated in a thermal vapour cell [3], in an atomic beam [4] and in ultracold atoms [5]. This detection technique has the advantage that it is continuous and can be performed in confined geometries down to the micron scale [6]. Consequently, one can envisage a compact electrometry device analogous to the chip scale atomic magnetometer [7].

Ladder EIT [8] involving a Rydberg state arises due to the formation of Rydberg dark states, which are coherent superpositions of the ground state and a Rydberg state. Rydberg dark resonances result in a narrow feature in the susceptibility, and thereby an enhanced electro-optic effect compared to bare Rydberg states [9]. This electro-optic effect can be measured either directly, by the displacement of the EIT dips in the absorption spectrum [3], or indirectly, by the phase shift of the probe field due to the electric-field dependence of the refractive index [9]. By reducing the probe laser intensity, the Rydberg population in the dark state can be made vanishingly small, while the change in transmission remains unchanged. Consequently, the effect of collisional ionization, which is often observed in high-density vapours [10], can be eliminated.

Possible applications of Rydberg dark states include single-photon entanglement [11], the generation of exotic entangled states [12] and mesoscopic quantum gates [13]. In addition, they are of interest for applications in electrometry because of their giant dc Kerr coefficient [9]. However, the sensitivity of a Rydberg dark state electrometer is limited by laser frequency fluctuations. Since reducing those to a suitable level entails a considerable experimental overhead, a technique to measure electric fields that is insensitive to the absolute laser frequency is desirable. Measurements of the splitting between D Stark sublevels [3] or between Stark states of higher angular momentum may be used to this end.

In this paper, we demonstrate the formation of Rydberg dark states dressed by a radio frequency (rf) field. Microwave or rf dressing of Rydberg states has previously been observed using laser excitation and field ionization of an atomic beam [14, 15] or of cold atoms [16]. Here, however, the resulting Floquet states are observed as EIT resonances in the absorption spectrum of the probe laser beam in a vapour cell. We show that these rf-dressed dark states have an enhanced sensitivity to dc electric fields. We also show that the strength of the dc electric field is encoded not only in the overall shift of the corresponding EIT feature, but also in the shape of the transparency window. As a consequence, and as we illustrate by an actual measurement, rf dressing may help determine the dc field without absolute knowledge of the laser frequency. In addition, we show how the line shape of the dark state resonance provides information about the electric field inhomogeneity within the interaction region.

2. Theory

We focus on EIT in the ladder system in which a weak probe laser (wavelength 780 nm) is scanned through resonance with the transitions from the ground $5S_{1/2}$, $F = 2$ state to the $5P_{3/2}$, $F' = (2, 3)$ states of ^{87}Rb, in the presence of both dc and ac electric fields and a coupling laser (wavelength 480 nm) resonant with the $5P_{3/2}$, $F' = 3$ to the $32S_{1/2}$, $F'' = 2$ transition. Such a ladder system is ideal for rf dressing as the two components of the dark state have a large differential shift in an external field and there is no additional splitting of the $J = 1/2$ Rydberg state.

At any point in the cell, the local applied electric field can be written as $\mathcal{E}(t) = \mathcal{E}_{\rm dc} + \mathcal{E}_{\rm ac} \sin \omega_{\rm m} t$. (The ac field and dc field have the same direction, and the angle between this direction and the polarization of the laser beams is inessential here, since the Rydberg state is of S-symmetry.) In the experiment, $\omega_{\rm m}/2\pi$ ranges from 10 to 30 MHz, which is much less than the relevant optical transition frequencies. Ignoring the laser fields and decoherence for the time being, we can work within the adiabatic approximation and describe each of the hyperfine components of the $32S_{1/2}$ state by a time-dependent state vector of the form [17]

$$|\Psi(t)\rangle = \exp\left(-\frac{\mathrm{i}}{\hbar}\int^{t} E[\mathcal{E}(t')]\,\mathrm{d}t'\right)|\psi[\mathcal{E}(t)]\rangle. \tag{1}$$

In this expression, $|\psi(\mathcal{E})\rangle$ is the Stark state that develops from the field-free state when a static field is adiabatically turned on from 0 to $\mathcal{E}$, and $E(\mathcal{E})$ is the corresponding eigenenergy of the Stark Hamiltonian. The dc and ac fields are sufficiently weak that one can take $E(\mathcal{E}) = E^{(0)} - (\alpha/2)\mathcal{E}^2$ and $|\psi(\mathcal{E})\rangle = |\psi^{(0)}\rangle + \mathcal{E}|\psi^{(1)}\rangle$, where α denotes the static dipole polarizability of the Rydberg state [18], and for each hyperfine component of the $32S_{1/2}$ state, $E^{(0)}$ and $|\psi^{(0)}\rangle$ are the energy and state vectors of this component in the absence of the field, and $|\psi^{(1)}\rangle$ is the first-order coefficient of the perturbative expansion of the Stark state $|\psi(\mathcal{E})\rangle$ in powers of $\mathcal{E}$. Since the field $\mathcal{E}(t)$ is monochromatic, the state vector of the rf-dressed Rydberg state can also be written in the Floquet–Fourier form

$$|\Psi(t)\rangle = \sum_{N=-\infty}^{\infty} \exp(-\mathrm{i}\epsilon_N t/\hbar)|\psi_N\rangle, \tag{2}$$

with $\epsilon_N = \epsilon_0 + N\hbar\omega_{\rm m}$. The harmonic components $|\psi_N\rangle$ and the energies ϵ_N are readily found by comparing equations (1) and (2) [15, 16]; using the approximate form of $E(\mathcal{E})$ mentioned

above, we obtain

$$\exp\left(-\frac{\mathrm{i}}{\hbar}\int^{t} E[\mathcal{E}(t')]\,\mathrm{d}t'\right) = \exp\left[-\frac{\mathrm{i}}{\hbar}\left(E^{(0)} - \frac{\alpha^2}{2}\mathcal{E}_{\mathrm{dc}}^2 - \frac{\alpha^2}{4}\mathcal{E}_{\mathrm{ac}}^2\right)t\right] B(x, y, \omega_{\mathrm{m}}t), \tag{3}$$

where $x = \alpha\mathcal{E}_{\mathrm{dc}}\mathcal{E}_{\mathrm{ac}}/(\hbar\omega_{\mathrm{m}})$, $y = \alpha\mathcal{E}_{\mathrm{ac}}^2/(8\hbar\omega_{\mathrm{m}})$ and

$$B(x, y, \omega_{\mathrm{m}}t) = \exp\left[-\mathrm{i}\left(x\cos\omega_{\mathrm{m}}t + y\sin 2\omega_{\mathrm{m}}t\right)\right]. \tag{4}$$

Expressions for the harmonic components $|\psi_N\rangle$ and the energies ϵ_N follow from expanding the function defined by equation (4) in a Fourier series and, in the right-hand side of equation (1), collating the terms oscillating with the same frequency. We obtain

$$\epsilon_N = E^{(0)} - \frac{\alpha^2}{2}\mathcal{E}_{\mathrm{dc}}^2 - \frac{\alpha^2}{4}\mathcal{E}_{\mathrm{ac}}^2 + N\hbar\omega_{\mathrm{m}} \tag{5}$$

and $|\psi_N\rangle = B_N|\psi^{(0)}\rangle + C_N|\psi^{(1)}\rangle$, with

$$B_N = \sum_{M=-\infty}^{\infty} \mathrm{i}^{N-2M} J_{2M-N}\left(\frac{\alpha\mathcal{E}_{\mathrm{dc}}\mathcal{E}_{\mathrm{ac}}}{\hbar\omega_{\mathrm{m}}}\right) J_M\left(\frac{\alpha\mathcal{E}_{\mathrm{ac}}^2}{8\hbar\omega_{\mathrm{m}}}\right) \tag{6}$$

and $C_N = B_N\mathcal{E}_{\mathrm{dc}} + (B_{N+1} - B_{N-1})\mathcal{E}_{\mathrm{ac}}/(2\mathrm{i})$. Hence, when decoherence is ignored, each of the two hyperfine components of the $32S_{1/2}$ state effectively turns into a manifold of equally spaced states under the action of the ac field [14]–[16]. Because the vectors $|\psi^{(0)}\rangle$ and $|\psi^{(1)}\rangle$ have opposite parity, $|\psi^{(1)}\rangle$ does not couple to the $5P_{3/2}$ state. Therefore, the Rabi frequency for the transition from a particular hyperfine component of this state to a particular component of the dressed Rydberg state differs from the corresponding zero-field Rabi frequency only by a factor $|B_N|$ (for the transition to the component with energy ϵ_N). The $5S_{1/2}$ and $5P_{3/2}$ states are also dressed by the applied field, but their polarizability is too small for any of their Floquet sideband states to be significantly populated at the ac field amplitudes considered here.

It follows that under the action of the ac field, and provided the relevant relaxation times are much longer than $2\pi/\omega_{\mathrm{m}}$, one should expect that the Rydberg dark states turn into Floquet manifolds of dark states and that each EIT dip in the absorption spectrum acquires multiple side bands. That such Floquet dark states can be obtained in conditions easily accessible to experiment is one of the results of this paper. (In the opposite limit, where the decoherence time is much shorter than the period of modulation, EIT happens as if the applied electric field is static and the experimental signal is the time average of the instantaneous absorption spectrum over the distribution of values of $\mathcal{E}(t)$).

3. Comparison between theory and experiment

The schematics of the experimental setup and of the energy levels scheme are shown in figure 1. We employ a specially fabricated 11-mm-long Rb vapour cell containing two parallel plane electrodes running along its whole length and separated by a 5 mm gap. The probe beam and the co-axial, counter-propagating coupling beam are directed along the electrode cell axis and are both polarized parallel to the electrodes. Each beam is focused using 10 cm lenses. The probe beam has an input power of 300 nW and a $1/\mathrm{e}^2$ radius of 1.7 mm at the centre of the cell. The corresponding values for the coupling beam are 40 mW and 1.0 mm. The latter is stabilized against slow drift using EIT in a reference cell [19]. The transmission through the electrode cell is monitored as a function of the probe detuning. To increase the number density

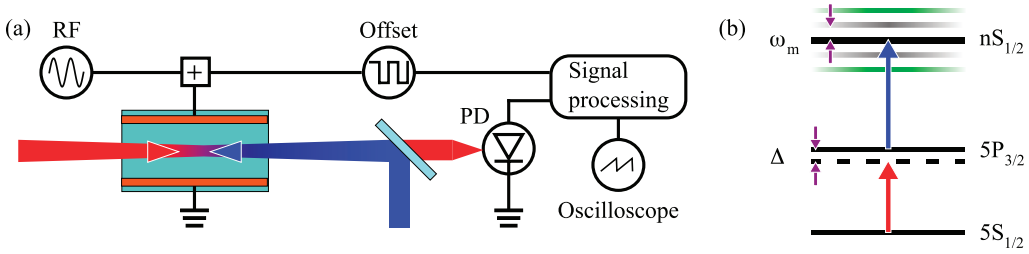

Figure 1. (a) Schematic of the experimental setup. The 780 nm probe beam (red) and 480 nm coupling beam (blue) counterpropagate through an Rb cell containing parallel plane electrodes. The rf ac field and the dc offset are applied by imposing a potential difference across the electrodes. The transmission of the probe beam through the cell is monitored on a photodiode. The photodiode signal is either detected directly or for the case of low-frequency modulation of the dc field using lock-in detection. (b) Schematic of the energy level scheme. The detuning Δ of the probe beam is varied. The coupling beam is resonant with the transition between the intermediate $5P_{3/2}$, $F' = 3$ state and the Rydberg $nS_{1/2}$, $F'' = 2$ state ($n = 32$). An applied electric field with angular frequency ω_m generates a ladder Floquet state separated by integer multiples of ω_m. The first-order Floquet dark states (grey) are particularly sensitive to any dc field.

of Rb atoms, the electrode cell is heated to about 40 °C. The probe beam is split into two, with one component propagating through the electrode cell and the other passing through a longer room temperature cell. By subtracting these two signals, the Doppler background is removed. Measuring the off-resonant probe beam power after the electrode cell allows the change in transmission, ΔT, to be calibrated. (ΔT is the difference between the transmitted power of the probe beam with the coupling beam acting and that in the absence of the coupling beam, divided by the transmitted power at a large detuning from resonance.) The detuning axis is calibrated using saturation/hyperfine pumping spectroscopy.

A typical EIT spectrum with an applied ac field is shown in figure 2, together with theoretical fits for different spatial profiles of the electric field. The theoretical model of EIT is based on the steady-state solution of the optical Bloch equations in the weak probe limit [20], assuming that the different magnetic sublevels of the ground state are equally populated. In the experiment, the intensity of the probe beam, $I \approx 3I_{sat}$, is considerably higher than the ideal weak probe limit [21]; however, good agreement can still be obtained. The absorption spectrum is obtained by integrating the absorption coefficient over the velocity distribution of the atoms, the spatial profiles of the two laser beams and the length of the cell. The absorption coefficient is a function of four parameters that must be derived from the data, namely the Rabi frequency for the $5P_{3/2}$, $F' = 3$ to $32S_{1/2}$, $F'' = 2$ transition, the dephasing rates of $5P_{3/2}$–$5S_{1/2}$ and $32S_{1/2}$–$5P_{3/2}$ coherences, and the temperature of the vapour. The values of these experimental parameters are obtained by a least-square fit of the theoretical change in transmission, ΔT, to the data. The fit covers a range of probe detunings encompassing both the $5P_{3/2}$, $F' = 2$ and $F' = 3$ states, whereas only the latter is shown in figure 2. The mean separation between the plates is not known with sufficient precision and therefore is derived

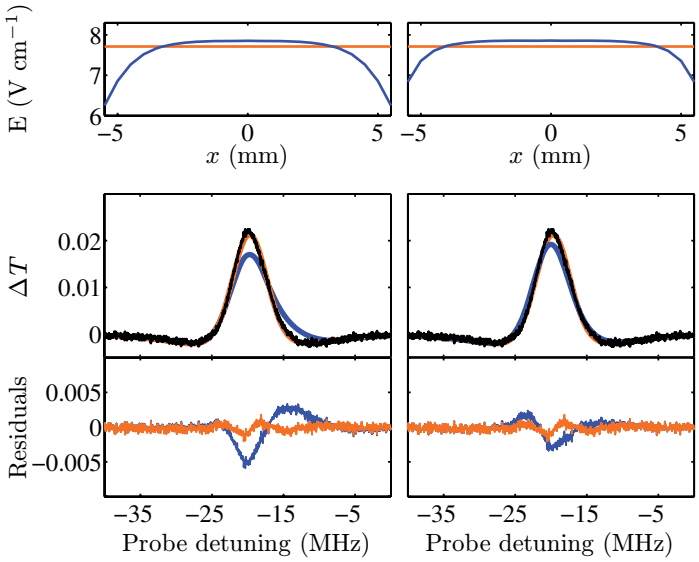

Figure 2. Comparison between the observed EIT spectra (black) for an applied ac electric field, $\mathcal{E}_{ac} = 7.7\,\mathrm{V\,cm^{-1}}$, and the theoretical EIT spectra calculated for the actual electrode geometry (blue) and for a uniform field (red). ΔT is the change in transmission, as defined in the text. The difference between the theoretical results and the data is shown in the bottom row of the figure. In the theoretical model, it is assumed either that the laser beams are aligned exactly on the longitudinal axis of the two electrodes (a), or that they are parallel to this axis but are offset by 1 mm towards one of the plates (b). The corresponding electric fields distributions are shown at the top. In this example, the electric field frequency is 26 MHz.

from the data by fitting the Stark shift of the EIT resonances to equation (5) for a number of different values of the applied voltage.

The spatial profile of the applied electric field along the laser beam axis is unknown due to the possibility of free charges inside the cell [3]. The field produced by the Stark plates drops significantly at their edges (see the top panels of figure 2). If we assume that the field experienced by the atoms exposed to the laser beams varies accordingly, the resulting theoretical EIT profile is asymmetric and inconsistent with the data (see the middle and bottom panels of figure 2). The theoretical results are found to be in good agreement with the data if the field is assumed to be uniform. This would occur if the free charges inside the cell equalize the electric field in the interaction region. We note, in this respect, that charges can be created by the photoelectric effect where the coupling laser intersects the Rb vapour on the inner surface of the cell, the photoelectrons being ejected from the surface. A net positive charge of $10^6 e$ on each window distributed over the waist of the coupling laser is sufficient to produce a total field with a spatial profile consistent with the experimentally observed line shape. We cannot exclude a misalignment of the laser beams with respect to the centre of the plates; however, the resulting offset would be less than 1 mm and even at 1 mm from the axis the field produced by the plates is still too inhomogeneous, in our model, to be compatible with the data (see the right-hand column of figure 2).

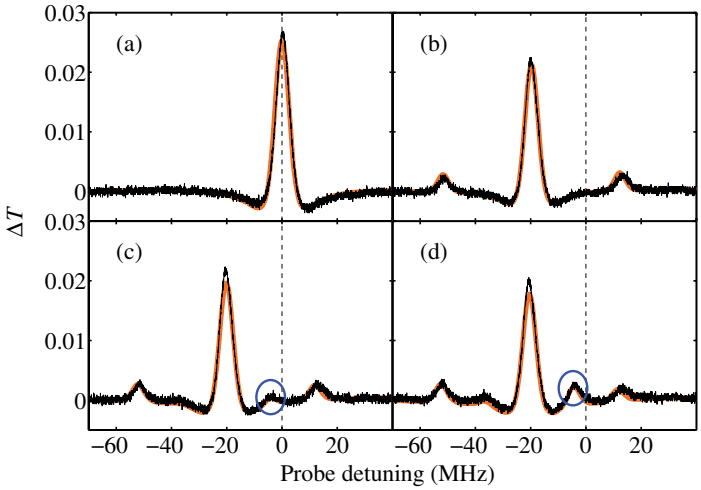

Figure 3. The effect of ac and dc electric fields on the Rydberg EIT spectrum. ΔT is the change in transmission defined in the text. The thick curves are theoretical predictions based on the solution of the steady-state optical Bloch equations. (a) Spectrum with no applied field. (b) Spectrum with an rf field with a frequency of 26 MHz ($\mathcal{E}_{ac} = 7.7\,\mathrm{V\,cm^{-1}}$). (c) and (d) Spectrum with the rf field plus a dc field; $\mathcal{E}_{dc} = 0.4\,\mathrm{V\,cm^{-1}}$ in (c) and $0.8\,\mathrm{V\,cm^{-1}}$ in (d). A circle is drawn around the +1 sideband in (c) and (d).

4. Observation of Floquet dark states

Following the analysis in the previous section, we assume that the electric field experienced by the atoms is homogeneous, and measure spectra for different combinations of ac and dc applied fields ($\mathcal{E}_{dc}$ and $\mathcal{E}_{ac}$). The results are presented in figure 3. The theoretical spectra are calculated assuming that the Rydberg state is described by the Floquet state vector (2) and that the Rabi frequency for the $5P_{3/2}$, $F' = 3$ to $32S_{1/2}$, $F'' = 2$ transition, the dephasing rates of $5P_{3/2}$–$5S_{1/2}$ and $32S_{1/2}$–$5P_{3/2}$ coherences and the temperature of the vapour, which, as mentioned in section 3, we derive from the data, have the same values as in the zero-field case.

In figure 3(b), we consider a case where only a pure ac field is applied. As compared to figure 3(a), the main EIT peak is shifted by the ac Stark effect and the EIT profile acquires sidebands at the second harmonics of the modulation frequency. The spacing between the sidebands and the carrier in the transmission spectrum is smaller than $2\omega_m/(2\pi)$ by a factor of 480/780 due to the Doppler mismatch. In view of the good agreement between theory and the measured data, we attribute the observed sidebands to the formation of Floquet dark states.

There are no odd-order sidebands in the absence of a dc field since $B_N = 0$ for odd values of N when $\mathcal{E}_{dc} = 0$. Their absence is consistent with the dipole selection rules, which forbid transitions from a P state to an S state by exchange of one laser photon and an odd number of rf photons. The effect of adding a weak dc offset is shown in figure 3(c). The spectrum acquires first-order sidebands, since $|\psi^{(0)}\rangle$ contributes to every $|\psi_n\rangle$ when $\mathcal{E}_{dc} \neq 0$. As can be seen by comparing figures 3(c) and (d), increasing the dc field modifies the EIT spectrum in several

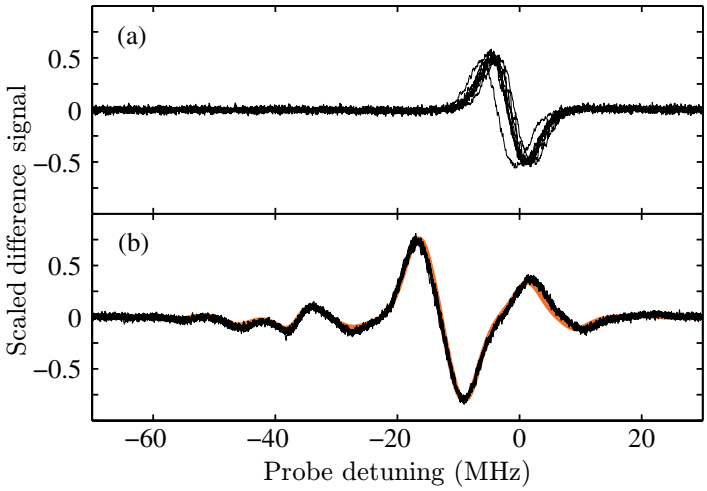

Figure 4. The dc field signal obtained by turning the dc field on and off at 50 kHz and using lock-in detection. The quantity shown is the difference between the change in transmission, ΔT, with and without the dc field, multiplied by a constant scaling factor to facilitate the comparison. This factor is chosen such that the difference signal in (a), averaged over all the datasets, varies between -0.5 and 0.5. The same factor is used in (b). (a) The difference signal measured for $\mathcal{E}_{ac} = 0$ and $\mathcal{E}_{dc} = 1.37\,\mathrm{V\,cm^{-1}}$. Ten datasets are presented; the results shown are not corrected for the frequency fluctuations of the probe laser. (b) The difference signal measured for $\mathcal{E}_{ac} = 7.14\,\mathrm{V\,cm^{-1}}$ and $\mathcal{E}_{dc} = 1.37\,\mathrm{V\,cm^{-1}}$. The modulation frequency is 15 MHz. As in (a), ten datasets are presented, but here they are corrected for the frequency fluctuations of the probe laser using the Floquet model. The thick curve shows the Floquet EIT result calculated for a value of $\mathcal{E}_{dc}$, ensuring an optimal fit between the model and one of the datasets.

ways. The largest change occurs on the +1 sideband. In contrast, the additional Stark shift in the position of the central peak, which would be the only effect of the increase in the dc field in the absence of the modulation, is almost invisible on the scale of the figure. The comparison demonstrates the enhanced dc field sensitivity of rf-dressed Rydberg dark states.

5. Enhanced electric field sensitivity of Floquet dark states

To further illustrate this enhancement effect, we now show that adding an ac modulation helps deduce the dc component of the electric field from the EIT resonance. The difference between transmission spectra measured with and without applying a dc field is shown in figure 4. Here, we apply a low-frequency modulation (50 kHz, i.e. much less than the ac modulation frequency of 26 MHz) of the dc field. The photodiode signal is then processed using a lock-in amplifier whose output corresponds to difference between the EIT signal with and without the dc field, i.e. the difference between the change in transmission, ΔT, with and without the dc field. This difference between the dc field shifted resonance and the unshifted resonance results in a derivative line shape, as shown in figure 4. Each thin black line shown in figure 4 gives the lock-in signal averaged over four consecutive scans. Subsequently, we refer to this lock-in signal

as the difference signal, as it corresponds to the change in transmission with and without the dc field. Figure 4(a) shows the difference signal in the absence of ac field for ten individual datasets. The spread in the data reflects the instability of the probe laser. Deriving $\mathcal{E}_{dc}$ from these results is hindered by the fact that only the position of the EIT feature on the frequency axis, and not its shape, varies significantly with the strength of the dc field. Due to the experimental uncertainty in the probe frequency, a value of $\mathcal{E}_{dc}$ cannot be obtained by fitting the model to the data from figure 4(a). However, the fit is possible when these data are augmented by the difference EIT signal arising from the $5P_{3/2}$, $F' = 2$ state and by frequency calibration data obtained by saturation spectroscopy. The theoretical difference signal is calculated using the same values of the Rabi frequency, dephasing rates and temperature, as in figure 3(a). We treat $\mathcal{E}_{dc}$ as an unknown parameter. For comparison with the theory, we correct the experimental results for random variations in the calibration of the probe frequency and of the signal by rescaling and shifting the origins of the respective axes. The corresponding offsets and scaling factors are found for each individual dataset, together with $\mathcal{E}_{dc}$, by fitting the rescaled experimental difference signal to the model. From the ten values of $\mathcal{E}_{dc}$ obtained in this way, we find that $\mathcal{E}_{dc} = 1.6 \pm 0.4\,\mathrm{V\,cm^{-1}}$. This value is in agreement with that derived from the dc voltage applied to the electrodes, $1.37 \pm 0.02\,\mathrm{V\,cm^{-1}}$, but it has a larger uncertainty.

A constant ac field is then added and the line shape is extracted once more (figure 4(b)). The lock-in detection still only detects changes in signal due to the dc field. In this case, for the same dc field, the difference signal is larger and contains more features. As the details of these features depend on $\mathcal{E}_{dc}$, the change in the spectrum because of the dc field is readily separated from the frequency fluctuations of the probe laser. Measuring $\mathcal{E}_{dc}$ is thus easier. The theoretical difference signal is calculated in the same way as in the absence of the rf field. We assume for $\mathcal{E}_{ac}$ the value derived from the voltage applied to the electrodes. From the ten values of $\mathcal{E}_{dc}$ obtained by fitting the data from figure 4(b) to the model, we find that $\mathcal{E}_{dc} = 1.36 \pm 0.04\,\mathrm{V\,cm^{-1}}$ (or $1.40 \pm 0.03\,\mathrm{V\,cm^{-1}}$ when the saturation spectroscopy data and the signal from $5P_{3/2}$, $F' = 2$ state are also taken into account). For these parameters, introducing an ac modulation thus reduces the uncertainty in the dc field measurement by one order of magnitude.

In the case considered in figure 4, the application of the ac field also increases the amplitude of the difference signal by about 50%. As shown in figure 5, larger enhancements (of up to 3) can be obtained for other combinations of dc fields and modulation frequencies.

6. Summary and outlook

In summary, we demonstrate continuous probing of the electric field inside an alkali vapour cell. We demonstrate the formation of Floquet dark states induced by the application of an ac field to a ladder system involving a highly polarizable Rydberg state, and show that these states display enhanced sensitivity to dc electric fields and provide information on the strength of the dc field independent of the laser frequency. Potentially, an ac modulation may thus facilitate the measurement of the local electric field inside a vapour cell, which is a relevant issue in the control of Rydberg–Rydberg interactions. The simple theory outlined above can be generalized to the case where the field splits the Rydberg state into several Stark components, thereby opening the possibility of using ac modulation to enhance the sensitivity of measurements based on the D states or on states of higher angular momentum. Our results suggest that charge imbalances in an enclosed vapour cell may cancel the spatial inhomogeneities of the field, and therefore for local field measurements the interaction region may need to be limited to a small

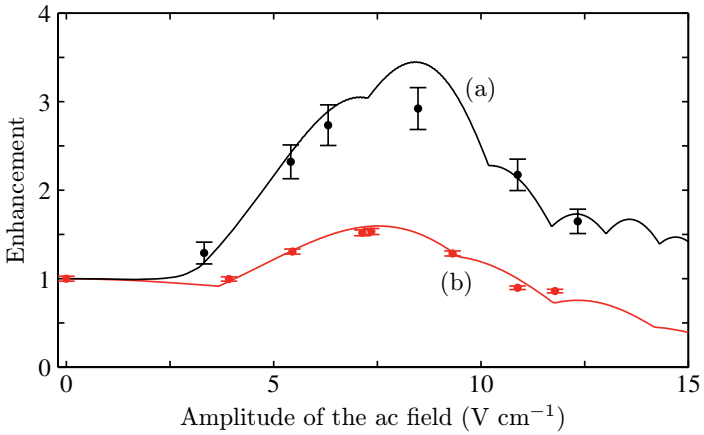

Figure 5. The increase in the amplitude of the dc electrometry signal as a function of $\mathcal{E}_{ac}$ (a) for a modulation frequency of 10 MHz and $\mathcal{E}_{dc} = 0.78$ V cm^{-1} and (b) for a modulation frequency of 15 MHz and $\mathcal{E}_{dc} = 1.37$ V cm^{-1}. The points are experimental data and the lines are the theoretical predictions of the model presented in the text. The sudden changes in the theoretical curves occur at zeros of the Bessel functions appearing in equation (6).

volume. This would be the case, for instance, in a three-photon Doppler-free excitation scheme in which the two pump and probe laser beams intersect at appropriate angles within a restricted volume. Three-photon excitation and optimizing the sensitivity of the electrometer will be the focus of future work.

Acknowledgments

We thank the EPSRC and the DPST Programme of the Thai Government for financial support.

References

[1] Gallagher T F 1994 *Rydberg Atoms* (Cambridge: Cambridge University Press)
[2] Osterwalder A and Merkt F 1999 *Phys. Rev. Lett.* **82** 1831
[3] Mohapatra A K, Jackson T R and Adams C S 2007 *Phys. Rev. Lett.* **98** 113003
[4] Mauger S, Millen J and Jones M P A 2007 *J. Phys. B: At. Mol. Opt. Phys.* **40** F319
[5] Weatherill K J, Pritchard J D, Abel R P, Bason M G, Mohapatra A K and Adams C S 2008 *J. Phys. B: At. Mol. Opt. Phys.* **41** 201002
[6] Kübler H, Shaffer J P, Baluksian T, Löw R and Pfau T 2009 arXiv:0908.0275
[7] Schwindt P D D, Knappe S, Shah V, Hollberg L, Kitching J, Liew L A and Moreland J 2004 *Appl. Phys. Lett.* **85** 6409
[8] Fleischhauer M, Imamoglu M and Marangos J P 2005 *Rev. Mod. Phys.* **77** 633
[9] Mohapatra A K, Bason M G, Butscher B, Weatherill K J and Adams C S 2008 *Nat. Phys.* **8** 890
[10] Keeler M L 2008 *Phys. Rev.* A **77** 034503
[11] Friedler I, Petrosyan D, Fleischhauer M and Kurizki G 2005 *Phys. Rev.* A **72** 043803
[12] Møller D, Madsen L B and Mølmer K 2008 *Phys. Rev. Lett.* **100** 170504
[13] Müller M, Lesanovsky I, Weimer H, Büchler H P and Zoller P 2009 *Phys. Rev. Lett.* **102** 170502

[14] Bayfield J E, Gardner L D, Gulkok Y Z and Sharma S D 1981 *Phys. Rev.* A **24** 138
van Linden van den Heuvell H B, Kachru R, Traa N H and Gallagher T F 1984 *Phys. Rev. Lett.* **53** 1901
[15] Zhang Y, Ciocca M, He L-W, Burkhardt C E and Leventhal J J 1994 *Phys. Rev.* A **50** 1101
[16] van Ditzhuijzen C S E, Tauschinsky A and van Linden van den Heuvell H B 2009 *Phys. Rev.* A **80** 063407
[17] Autler S H and Townes C H 1955 *Phys. Rev.* **100** 703
Pont M, Potvliege R M, Shakeshaft R and Teng Z-J 1992 *Phys. Rev.* A **45** 8235
[18] O'Sullivan M S and Stoicheff B P 1985 *Phys. Rev.* A **31** 2718
[19] Abel R P, Mohapatra A K, Bason M G, Pritchard J D, Weatherill K J, Raitzsch U and Adams C S 2009 *Appl. Phys. Lett.* **94** 071107
[20] Gea-Banacloche J, Li Y Q, Jin S Z and Xiao M 1995 *Phys. Rev.* A **51** 576
[21] Siddons P, Adams C S, Ge C and Hughes I G 2008 *J. Phys. B: At. Mol. Opt. Phys.* **41** 155004